

Multi-wavelength study of the pre-eruption dip in the recurrent nova T Coronae Borealis preceding imminent nova eruption

Songpeng Pei¹, Xiaowan Zhang¹, Renzhi Su², Yongzhi Cai^{3,4,5}, Ziwei Ou⁶, Qiang Li^{7,8}, Xiaoqin Ren^{7,8}, Taozhi Yang⁹, and Mingyue Li^{7,8}

¹ School of Physics and Electrical Engineering, Liupanshui Normal University, Liupanshui, Guizhou, 553004, China
e-mail: songpengpei@outlook.com

² Shanghai Astronomical Observatory, Chinese Academy of Sciences, 80 Nandan Road, Shanghai 200030, China

³ Yunnan Observatories, Chinese Academy of Sciences, Kunming 650216, China

⁴ International Centre of Supernovae, Yunnan Key Laboratory, Kunming 650216, China

⁵ Key Laboratory for the Structure and Evolution of Celestial Objects, Chinese Academy of Sciences, Kunming 650216, China

⁶ Tsung-Dao Lee Institute, Shanghai Jiao Tong University, Shanghai 201210, China

⁷ School of Physics and Electronic Science, Qiannan Normal University for Nationalities, Duyun 558000, China

⁸ Qiannan Key Laboratory of Radio Astronomy, Guizhou Province, Duyun 558000, China

⁹ Ministry of Education Key Laboratory for Nonequilibrium Synthesis and Modulation of Condensed Matter, School of Physics, Xi'an Jiaotong University, 710049 Xi'an, China

Received 00.00.2025; accepted 00.00.2025

ABSTRACT

We present a multi-wavelength study of the symbiotic recurrent nova (RN) T Coronae Borealis (T CrB) using Swift Burst Alert Telescope (BAT)/ X-Ray Telescope (XRT) / UltraViolet Optical Telescope (UVOT) and American Association of Variable Stars Observers (AAVSO) observations from 2005 to 2025. Our analysis spans quiescent, high, and pre-eruption dip states. We find that brightening amplitudes increase toward shorter wavelengths in both optical and UV bands, while the UV and X-ray fluxes are generally anti-correlated throughout all phases. During the 2023–2024 pre-eruption dip, soft and hard X-rays increased as optical and ultraviolet (UV) brightness declined, consistent with a transition from an optically thick to thin boundary layer driven by a reduction in the accretion rate. We also report, for the first time, a second, lower-amplitude dip occurring between September 2024 and February 2025 following the primary 2023–2024 pre-eruption dip. The observed variability supports an accretion-variation scenario as a unifying explanation for both the high and dip states, and may signal an imminent nova eruption.

Key words. accretion, accretion disks — stars: binaries: symbiotic — stars: novae, cataclysmic variables — stars: individual (T CrB) — stars: white dwarfs — X-rays: binaries

1. Introduction

T Coronae Borealis (T CrB; HR 5958; HD 143454) is the nearest known RN and one of the brightest and most studied in this class. It has had recorded eruptions in 1866 and 1946, each peaking at about $V \approx 2.0$ (Sanford 1949). There are also possible historical eruptions in AD 1217 and 1787 (Schaefer 2023b; Schaefer et al. 2023). After ~ 80 years of quiescence since 1946, the next nova eruption is widely predicted to occur imminently (Munari et al. 2016; Ilkiewicz et al. 2023; Maslenikova et al. 2023; Zamanov et al. 2023; Merc et al. 2025), and current estimates place it in the 2023.0–2026.8 range (Luna et al. 2020; Schaefer et al. 2023; Schaefer 2023a). In general, recurrent novae (RNe) are rare (only ~ 11 are known in the Milky Way), and T CrB is the nearest of the four known symbiotic RNe. This imminent outburst could become the brightest nova of the modern era.

T CrB comprises a Roche lobe-filling M4 III red giant ($M = 0.69^{+0.02}_{-0.01} M_{\odot}$, $R = 65 \pm 6 R_{\odot}$) (Belczynski & Mikolajewska 1998; Mürset & Schmid 1999; Hinkle et al. 2025) and a extremely massive white dwarf (WD; $M_{WD} = 1.37 \pm 0.01 M_{\odot}$; (Hinkle et al. 2025)). The orbital period is 227.57–227.58 d (Fekel et al. 2000; Schaefer 2023a; Planquart et al. 2025), and the V -band light curve shows a 0.3 mag ellipsoidal modulation

at half the orbital period (Bailey 1975; Schaefer 2023a). The distance is estimated as 896 ± 22 pc¹ from *Gaia* early data release 3 (eDR3) (Bailer-Jones et al. 2021). Schaefer (2022) estimated a similar distance of ~ 914 pc. T CrB has also been suggested to display dwarf-nova-like outbursts under some conditions (Ilkiewicz et al. 2023).

Since its 1946 nova event, T CrB has alternated between long quiescent intervals and episodes of enhanced activity. Around 2014–2015 the system suddenly brightened: in 2015 it entered a so-called super-active state² akin to that seen in the few years before the 1946 eruption (Munari et al. 2016; Ilkiewicz et al. 2016; Luna et al. 2018). During this high state the star’s UV, optical, and radio brightness increased dramatically; the usual orbital modulation in the B band disappeared; strong high-ionization emission lines appeared in the spectrum; and the hard X-ray flux all but vanished (Munari et al. 2016; Luna et al. 2018; Linford et al. 2019). It has been suggested that this high state may be driven by a SU UMa-type dwarf-nova mechanism (Ilkiewicz et al. 2023). This unusual behavior

¹ <http://dc.g-vo.org/tableinfo/gedr3dist.main>

² Throughout this text, the term *high* state refers to the period of heightened activity in T CrB that began in 2014–2015 and ended in 2023

has been suggested as a possible precursor of the next nova eruption (Munari et al. 2016; Luna et al. 2020; Schaefer 2023a; Ilkiewicz et al. 2023; Zamanov et al. 2023).

By mid-2023 the high state was clearly winding down (Munari 2023; Teyssier et al. 2023): the optical luminosity fell from about $20 - 25 L_{\odot}$ in April–May 2023 to $\sim 8 - 9 L_{\odot}$ by August (Zamanov et al. 2023). In April 2023 the system entered a pre-eruption dip state³ (Schaefer et al. 2023; Kuin et al. 2023), as had been predicted by Schaefer (2023a). In this dip, the optical and UV flux declined noticeably – a behavior reminiscent of the fading seen before the 1946 nova eruption. Like the high state, the 2023 dip was proposed as a potential precursor to the forthcoming nova eruption (Schaefer 2023a; Schaefer et al. 2023; Toone 2023; Kuin et al. 2023).

However, Merc et al. (2025) have shown that the 2023–2024 pre-eruption dip only partially resembled the 1946 event. In particular, the dip matched the 1946 behavior in the B band but not in the V band, leading them to argue that it may not reliably predict the nova timing. These deviations imply that the next nova eruption could occur somewhat earlier or later than the date predicted based on the pre-eruption dip (Schaefer et al. 2023). In any case, the 2023–2024 pre-eruption dip – observed in detail with modern multiwavelength instrumentation – offers valuable insight into the accretion physics of this symbiotic RN.

T CrB thus occupies a unique niche among interacting binaries. It shows features of RNe, symbiotic stars, cataclysmic variables, and dwarf novae all at once. Its near-Chandrasekhar-limit WD, together with phenomena such as the high state, the pre-eruption dip, and the post-nova secondary maximum, make it an important laboratory for studying accretion in long-period WD binaries. In particular, constraining its behavior helps inform models of binary evolution leading to Type Ia supernovae (Shahbaz et al. 1997; Fekel et al. 2000; Hachisu & Kato 2001; Liu et al. 2019).

The high state observed between 2014 and 2023 has been extensively studied (e.g., Munari et al. 2016; Ilkiewicz et al. 2016; Zhekov & Tomov 2019; Linford et al. 2019; Luna et al. 2020; Zamanov et al. 2023; Munari 2023; Schaefer 2023a; Ilkiewicz et al. 2023; Stoyanov et al. 2025; Merc et al. 2025; Planquart et al. 2025; Schlindwein et al. 2025). In this paper we analyze archival X-ray, optical, and UV observations of T CrB from 2005–2025 (spanning the quiescent, high, and pre-dip states) in order to investigate the nature of the pre-eruption dip. Our goal is to use this multiwavelength dataset to shed light on the accretion processes and impending nova behavior of this iconic symbiotic RN.

The UVW1, UVM2, and UVW2 filter data from Swift/UVOT used in this study were previously analyzed by Munari et al. (2025). Portions of the Swift/XRT dataset have been examined by Kennea et al. (2009); Ilkiewicz et al. (2016); Luna et al. (2018); Zhekov & Tomov (2019), while segments of the Swift/BAT observations were analyzed by Luna et al. (2018). In this paper, we build on these works by presenting new findings on the iconic and extensively studied RN T CrB. In Sect. 1, we provide a brief introduction to T CrB. In Section 2, we review the details of the observations and the data reduction process. In Section 3, we present results from analysis of the X-ray, optical, and UV emission of T CrB. In Section 4, we discuss our findings and Section 5 presents our summary and conclusions.

³ Throughout this text, the term *pre-eruption dip* refers to the phase of T CrB’s activity that began in 2023 and ended in 2024

2. Observation and data reduction

The Neil Gehrels Swift Observatory (hereafter, *Swift*; Gehrels et al. 2004) began observing T CrB on 2005-06-17. T CrB was monitored with the Swift using all three instruments: the XRT (Burrows et al. 2005), the BAT (Barthelmy et al. 2005), and the UVOT (Roming et al. 2005). We used Swift observations from 2005-06-17 to 2025-05-03 (MJD 53538–60798), comprising 278 pointed observations (total XRT exposure: 437.3 ks), as shown in Table 1. The XRT monitoring operated exclusively in Photon Counting (PC) mode. Raw XRT event files were processed with FTOOLS package in HEASOFT v. 6.30.1⁴ using the xrtpipeline task and the latest calibration files. Source events were then extracted with XSELECT from a circular region of radius 20 pixels centered on the SIMBAD coordinates of T CrB, and background events were taken from a nearby source-free region. The resulting XRT count rates were corrected for vignetting and bad CCD columns using the XRTLCORR tool. The processed BAT data obtained from the Swift BAT transient monitor page was also used (Krimm et al. 2013). These BAT data extend the hard X-ray coverage and trace the long-term high-energy behavior of the system.

Simultaneously, each Swift pointing included UVOT exposures. During 99 observations the Swift UVOT (Roming et al. 2005) was in the event mode, providing fast photometry in the UVM2 filter (90 observations) and UGRISM filter (9 observations). Swift UVOT was in the image mode in the rest 179 observations, providing the mean magnitude of each observation in one or more of the six UVOT filters (V, B, U, UVW1, UVM2 and UVW2). All the Swift UVOT data were processed by using the FTOOLS package. UVOT data were reduced using the standard HEASoft/UVOT pipeline. Source brightness and count rates were extracted with uvotsource using a 5"-radius aperture, with the background estimated from a nearby sky region. Some UVOT frames were saturated (source brighter than around 10–11 mag), so for those exposures we measured the brightness using the read-out streak method (Page et al. 2013). Because the Swift/UVOT UVW2 filter is affected by a significant red leak, and T CrB has a bright, very red component from its red giant companion, the leaked optical light dominates the UV signal—especially during quiescent and pre-eruption dip states. Consequently, the UVW2 light curve presented here is included for reference only.

The logs of all the observations with the date, exposure time and mean count rate are compiled in Table 1.

The high-energy observations were supplemented with long-term optical photometry from the AAVSO. We retrieved all publicly available I, R, V, B and U bands observations of T CrB from the AAVSO International Database, covering roughly 2005–2025 (~ 7400 days).

All timing data (X-ray) were referred to the Solar System barycenter (SSB) using the FTOOLS barycorr task. The multi-instrument data set (Swift XRT/BAT/UVOT plus AAVSO photometry) thus provides a well-calibrated, contemporaneous record of T CrB activity prior to its expected nova outburst.

3. Multi-wavelength variability and timing analysis

3.1. Evolution of optical, UV, and X-ray light curves

A comparison of T CrB’s variability across optical, UV, and X-ray energy ranges is presented in Fig. 1 and Fig. 2. Fig. 2 displays

⁴ <https://heasarc.gsfc.nasa.gov/docs/software/lheasoft/download.html>

Table 1. Log of all Swift XRT (PC mode) observations of T CrB between 2005.06 and 2025.05.

ObsID	Date ^a	Exp. (s)	Count rate
00035171001	53538.42	8822.9	0.075 ± 0.009
00035171002	53650.70	5185.6	0.080 ± 0.006
00035171003	53662.33	10325.2	0.101 ± 0.004
00035171004	54538.42	4033.8	0.109 ± 0.007
00035171005	54540.06	4876.8	0.099 ± 0.005
00035171006	54541.99	4080.5	0.101 ± 0.006
00045776001	55892.82	2730.3	0.063 ± 0.005
00045776002	55899.40	1236.1	0.101 ± 0.010
00081659001	57288.40	8255.7	0.063 ± 0.003
00081659002	57289.12	1657.3	0.071 ± 0.008
00045776003	57296.06	193.0	0.023 ± 0.005
00045776005	57771.52	10023.8	0.012 ± 0.001
00045776006	57783.37	9390.9	0.016 ± 0.002
00045776007	57792.74	475.9	0.019 ± 0.009
00045776008	57793.51	3269.8	0.018 ± 0.003
00045776009	57794.91	1313.8	0.023 ± 0.005
00045776010	57797.16	1125.9	0.026 ± 0.006
00045776011	57802.58	7092.9	0.015 ± 0.002
00045776012	57806.93	987.9	0.011 ± 0.004
00045776014	57815.63	498.7	0.010 ± 0.007
00045776015	57820.90	2810.7	0.014 ± 0.003
00045776016	57824.82	5390.3	0.015 ± 0.002
00045776017	57834.52	2663.1	0.012 ± 0.003
00045776018	57850.68	3882.3	0.007 ± 0.002
00045776019	57863.12	238.2	0.017 ± 0.012
00045776020	57864.93	4021.0	0.011 ± 0.002
00045776021	57885.48	3791.8	0.006 ± 0.002
00045776022	57932.74	3557.9	0.012 ± 0.002
00045776023	57952.68	3919.9	0.007 ± 0.002
00045776024	57987.44	1458.5	0.016 ± 0.004
00045776025	57988.91	1524.4	0.019 ± 0.005
00045776026	58022.53	4022.3	0.019 ± 0.003
00045776027	58053.45	743.3	0.005 ± 0.004
00045776028	58055.25	1697.4	0.009 ± 0.003
00045776029	58122.07	3640.3	0.016 ± 0.002
00045776030	58174.40	4068.4	0.004 ± 0.001
00045776031	58257.56	5067.3	0.009 ± 0.002
00045776032	58326.26	556.7	0.008 ± 0.002
00045776036	58391.61	461.3	0.013 ± 0.002
00045776038	58471.73	807.3	0.007 ± 0.001
00045776040	58548.50	656.9	0.010 ± 0.002
00011405001	58623.67	366.7	0.008 ± 0.002
00045776042	58668.57	268.2	0.025 ± 0.005
00045776044	58671.89	213.0	0.021 ± 0.005
00011548001	58730.38	366.0	0.010 ± 0.002
00012011001	58754.55	396.1	0.005 ± 0.002
00013032002	58839.51	1459.2	0.016 ± 0.004
00013032003	58842.04	280.8	0.013 ± 0.003
00013294047	58929.42	398.6	0.013 ± 0.003
00013559001	59011.34	353.5	0.019 ± 0.003
00013558002	59044.37	396.5	0.023 ± 0.003
00013558004	59072.22	446.3	0.022 ± 0.004
00089009001	59100.70	2808.9	0.011 ± 0.002
00013922001	59189.04	195.6	0.007 ± 0.003
00014166005	59287.69	142.9	0.038 ± 0.007
00014166007	59289.94	183.0	0.030 ± 0.006
00014166009	59290.67	223.1	0.020 ± 0.005
00014379001	59381.47	290.8	0.034 ± 0.006
00012011005	59405.37	150.4	0.011 ± 0.005
00012011007	59411.57	411.2	0.032 ± 0.005
00012011009	59439.16	160.5	0.010 ± 0.007
00012011011	59442.34	178.0	0.011 ± 0.004
00014765003	59443.53	153.0	0.011 ± 0.004
00014765005	59447.06	225.6	0.032 ± 0.006

Notes: ^a Modified Julian Date. The count rates were measured in the 0.3–10.0 keV.

Table 1. Continued. Log of all Swift XRT (PC mode) observations of T CrB between 2005.06 and 2025.05.

ObsID	Date ^a	Exp. (s)	Count rate
00012011013	59450.11	203.2	0.031 ± 0.008
00013558010	59646.60	152.9	0.020 ± 0.007
00013558012	59646.99	1053.0	0.012 ± 0.004
00013558013	59649.06	223.0	0.016 ± 0.005
00013558016	59721.49	581.4	0.029 ± 0.011
00013558017	59752.33	198.1	0.010 ± 0.005
00013558021	59782.49	195.6	0.029 ± 0.006
00013558023	59790.12	193.1	0.038 ± 0.008
00013558026	59791.31	163.0	0.027 ± 0.006
00013558028	59793.50	225.7	0.005 ± 0.003
00013558030	59798.48	178.0	0.022 ± 0.007
00013558032	59923.21	82.2	0.019 ± 0.005
00013558034	59923.31	1281.2	0.023 ± 0.005
00013558036	59923.68	218.1	0.017 ± 0.005
00013558035	59923.81	792.4	0.024 ± 0.006
00013558040	59954.09	1043.0	0.030 ± 0.006
00013558038	59954.15	188.2	0.043 ± 0.009
00013558042	59954.69	165.5	0.020 ± 0.005
00013558041	59954.75	712.1	0.016 ± 0.006
00013558046	59985.58	1211.1	0.051 ± 0.005
00013558044	59986.34	233.2	0.027 ± 0.006
00013558053	60013.68	744.7	0.035 ± 0.009
00013558052	60014.68	1023.0	0.070 ± 0.014
00013558056	60044.32	1547.0	0.044 ± 0.005
00013558059	60044.58	937.7	0.073 ± 0.013
00013558057	60044.66	682.0	0.092 ± 0.013
00013558060	60074.30	218.1	0.033 ± 0.011
00013558065	60074.89	403.7	0.018 ± 0.009
00013558067	60076.79	461.3	0.042 ± 0.015
00013558068	60080.50	1459.3	0.016 ± 0.004
00013558069	60089.75	105.3	0.013 ± 0.010
00013558072	60089.97	747.2	0.004 ± 0.007
00013558077	60104.45	1353.8	0.025 ± 0.005
00013558083	60119.33	1441.7	0.023 ± 0.005
00013558081	60119.45	170.5	0.019 ± 0.009
00013558087	60119.72	275.8	0.023 ± 0.008
00013558084	60119.78	646.9	0.031 ± 0.009
00013558091	60134.09	1373.5	0.013 ± 0.004
00013558089	60134.19	135.4	0.025 ± 0.007
00013558093	60134.73	228.2	0.012 ± 0.005
00013558092	60134.98	491.5	0.030 ± 0.010
00013558095	60149.25	130.4	0.004 ± 0.004
00013558098	60149.59	777.3	0.002 ± 0.003
00013558101	60149.66	195.6	0.010 ± 0.004
00013558103	60150.52	1338.0	0.012 ± 0.004
00013558106	60164.40	1502.2	0.107 ± 0.006
00013558110	60178.44	1562.0	0.087 ± 0.007
00013558116	60178.88	208.1	0.043 ± 0.008
00013558118	60191.55	1073.1	0.124 ± 0.012
00013558121	60192.08	504.0	0.153 ± 0.019
00013558124	60192.15	180.5	0.130 ± 0.017
00013558126	60192.54	170.5	0.124 ± 0.012
00013558128	60206.16	1393.6	0.119 ± 0.010
00013558131	60206.42	1451.7	0.122 ± 0.013
00013558132	60209.06	62.7	0.109 ± 0.016
00013558136	60220.49	1537.0	0.147 ± 0.007
00013558148	60234.43	152.9	0.130 ± 0.016
00013558147	60234.62	586.7	0.099 ± 0.015
00013558144	60234.81	1075.6	0.095 ± 0.011
00013558150	60234.88	140.4	0.082 ± 0.010
00013558153	60245.05	268.3	0.084 ± 0.006
00013558152	60245.48	817.5	0.053 ± 0.004
00013558158	60276.21	198.1	0.064 ± 0.008
00013558160	60276.63	1737.1	0.105 ± 0.006

Notes: ^a Modified Julian Date. The count rates were measured in the 0.3–10.0 keV.

Table 1. Continued. Log of all Swift XRT (PC mode) observations of T CrB between 2005.06 and 2025.05.

ObsID	Date ^a	Exp. (s)	Count rate
00013558164	60290.26	185.2	0.107 ± 0.015
00013558168	60290.84	183.2	0.079 ± 0.009
00013558167	60290.92	819.9	0.045 ± 0.009
00013558170	60304.03	255.7	0.169 ± 0.017
00013558174	60304.10	250.7	0.099 ± 0.017
00013558173	60304.82	661.9	0.058 ± 0.010
00013558176	60318.35	208.1	0.055 ± 0.013
00013558180	60318.76	195.6	0.100 ± 0.010
00013558185	60332.07	812.4	0.106 ± 0.013
00013558189	60332.33	892.6	0.093 ± 0.012
00013558182	60332.53	1328.9	0.053 ± 0.009
00013558188	60332.92	917.7	0.044 ± 0.008
00013558191	60346.11	205.6	0.054 ± 0.012
00013558193	60346.78	498.9	0.092 ± 0.016
00013558194	60346.84	200.6	0.031 ± 0.011
00013558202	60362.14	438.8	0.069 ± 0.017
00013558200	60362.78	152.9	0.091 ± 0.014
00013558204	60376.36	183.0	0.068 ± 0.011
00013558206	60376.82	1381.5	0.090 ± 0.007
00097564001	60411.01	92.8	0.085 ± 0.016
00097564005	60411.73	178.0	0.051 ± 0.011
00097564004	60411.86	897.6	0.051 ± 0.009
00097564009	60421.53	769.7	0.032 ± 0.008
00097564014	60421.87	100.3	0.029 ± 0.009
00097564016	60431.21	125.4	0.017 ± 0.005
00097564015	60431.42	939.9	0.067 ± 0.010
00097564018	60431.74	183.0	0.036 ± 0.007
00097564021	60441.41	160.5	0.047 ± 0.009
00097564020	60441.49	860.0	0.103 ± 0.013
00097564023	60441.62	897.6	0.029 ± 0.012
00097564024	60441.81	162.8	0.042 ± 0.015
00097564027	60451.48	213.1	0.078 ± 0.009
00097564029	60451.81	123.0	0.068 ± 0.008
00097564026	60451.87	1501.9	0.110 ± 0.011
00097564033	60461.35	190.5	0.102 ± 0.011
00097564031	60461.49	952.8	0.122 ± 0.013
00097564035	60461.74	190.5	0.108 ± 0.027
00097564036	60461.75	957.8	0.099 ± 0.019
00097564037	60471.28	195.6	0.094 ± 0.011
00097564041	60471.54	163.0	0.053 ± 0.008
00097564040	60471.67	718.8	0.074 ± 0.012
00097564039	60471.80	890.1	0.081 ± 0.011
00097564043	60481.34	144.1	0.060 ± 0.009
00097564045	60481.40	865.0	0.048 ± 0.009
00097564047	60481.55	195.6	0.058 ± 0.009
00097564046	60481.73	265.8	0.014 ± 0.011
00097564049	60491.33	165.5	0.114 ± 0.012
00097564051	60491.40	967.8	0.082 ± 0.011
00097564053	60491.66	165.5	0.070 ± 0.009
00097564052	60491.86	927.7	0.034 ± 0.007
00097564058	60501.40	581.7	0.027 ± 0.015
00097564057	60501.46	863.8	0.051 ± 0.016
00097564059	60501.72	120.3	0.046 ± 0.008
00097564064	60511.31	743.6	0.021 ± 0.008
00097564061	60511.38	205.6	0.049 ± 0.009
00097564065	60511.65	117.8	0.063 ± 0.012
00097564063	60511.78	885.1	0.045 ± 0.010
00097564069	60521.31	882.6	0.024 ± 0.006
00097564067	60521.38	160.6	0.051 ± 0.010
00097564070	60521.44	819.9	0.044 ± 0.008
00097564071	60521.97	240.7	0.055 ± 0.010
00097564073	60531.02	117.8	0.014 ± 0.006
00097564076	60531.35	423.0	0.018 ± 0.009
00097564077	60531.68	195.6	0.019 ± 0.006

Notes: ^a Modified Julian Date. The count rates were measured in the 0.3 – 10.0 keV.

Table 1. Continued. Log of all Swift XRT (PC mode) observations of T CrB between 2005.06 and 2025.05.

ObsID	Date ^a	Exp. (s)	Count rate
00097564075	60531.82	920.2	0.013 ± 0.005
00097564082	60541.20	60.2	0.014 ± 0.005
00097564084	60541.27	769.7	0.043 ± 0.009
00097564085	60541.33	777.3	0.012 ± 0.005
00097564086	60541.60	55.2	0.019 ± 0.010
00089722001	60546.79	1912.0	0.025 ± 0.004
00097564088	60551.05	937.8	0.022 ± 0.006
00097564093	60551.12	225.6	0.033 ± 0.010
00097564091	60551.51	208.0	0.017 ± 0.005
00097564089	60551.59	910.1	0.024 ± 0.006
00097564094	60561.29	72.7	0.077 ± 0.044
00097564096	60561.44	303.4	0.033 ± 0.021
00097564098	60561.70	155.4	0.021 ± 0.008
00097564111	60571.07	72.7	0.014 ± 0.006
00097564107	60571.46	621.8	0.030 ± 0.008
00097564105	60571.53	75.2	0.019 ± 0.006
00097564109	60571.85	824.9	0.023 ± 0.006
00097564112	60581.24	168.0	0.046 ± 0.008
00097564114	60581.38	930.2	0.019 ± 0.006
00097564115	60581.44	877.4	0.035 ± 0.007
00097564116	60581.70	135.4	0.022 ± 0.007
00097564120	60591.06	1100.7	0.026 ± 0.006
00097564118	60591.19	142.9	0.018 ± 0.010
00097564122	60591.65	102.8	0.015 ± 0.011
00097564121	60591.72	952.8	0.011 ± 0.005
00097564124	60601.03	188.2	0.009 ± 0.006
00097564126	60601.56	1073.1	0.021 ± 0.005
00097564128	60601.95	198.0	0.017 ± 0.008
00097564132	60611.05	887.6	0.015 ± 0.005
00097564133	60611.38	702.0	0.027 ± 0.007
00097564130	60611.45	73.6	0.029 ± 0.010
00097564134	60611.59	40.3	0.025 ± 0.009
00097564138	60643.19	170.5	0.022 ± 0.008
00097564136	60643.51	895.1	0.018 ± 0.006
00097564140	60643.91	135.4	0.013 ± 0.008
00097564137	60643.98	952.8	0.030 ± 0.007
00097564144	60653.19	137.9	0.031 ± 0.011
00097564143	60653.32	727.1	0.031 ± 0.014
00097564147	60653.86	293.3	0.052 ± 0.017
00097564142	60653.91	870.0	0.047 ± 0.010
00097564150	60663.26	140.4	0.034 ± 0.013
00097564152	60663.71	208.1	0.025 ± 0.010
00097564149	60663.85	920.2	0.030 ± 0.007
00097564148	60663.98	852.5	0.025 ± 0.006
00097564159	60673.66	298.0	0.025 ± 0.012
00097564155	60673.73	832.4	0.017 ± 0.007
00097564154	60673.79	865.0	0.029 ± 0.011
00097564162	60683.12	120.3	0.027 ± 0.010
00097564161	60683.18	1074.0	0.020 ± 0.005
00097564165	60683.52	997.9	0.011 ± 0.009
00097564160	60683.65	990.4	0.015 ± 0.005
00097564169	60693.24	210.6	0.029 ± 0.010
00097564168	60693.38	887.6	0.026 ± 0.006
00097564171	60693.77	265.8	0.024 ± 0.009
00097564167	60693.84	962.8	0.016 ± 0.005
00097564175	60703.04	218.1	0.010 ± 0.005
00097564174	60703.10	872.6	0.024 ± 0.006
00097564181	60713.09	130.4	0.035 ± 0.013
00097564183	60713.80	180.5	0.050 ± 0.011
00097564180	60713.88	614.3	0.049 ± 0.010
00097564179	60713.94	616.8	0.087 ± 0.013
00097564187	60723.07	223.1	0.022 ± 0.007
00097564186	60723.67	779.8	0.031 ± 0.007
00097564189	60723.92	283.3	0.035 ± 0.008

Notes: ^a Modified Julian Date. The count rates were measured in the 0.3–10.0 keV.

Table 1. Continued. Log of all Swift XRT (PC mode) observations of T CrB between 2005.06 and 2025.05.

ObsID	Date ^a	Exp. (s)	Count rate
00097564185	60723.99	918.8	0.022 ± 0.006
00097564193	60733.44	147.9	0.027 ± 0.006
00097564191	60733.51	1113.2	0.061 ± 0.008
00097564195	60733.69	188.1	0.041 ± 0.008
00097564192	60733.76	799.0	0.064 ± 0.010
00097564199	60743.02	27.6	0.029 ± 0.007
00097564198	60743.16	932.7	0.027 ± 0.006
00097564197	60743.22	920.2	0.027 ± 0.006
00097564205	60753.37	155.4	0.034 ± 0.008
00097564204	60753.70	877.6	0.013 ± 0.005
00097564207	60753.77	90.3	0.016 ± 0.008
00097564203	60753.84	950.3	0.013 ± 0.005
00097564212	60763.02	147.9	0.035 ± 0.022
00097564213	60763.73	93.4	0.038 ± 0.012
00097564210	60763.87	950.3	0.043 ± 0.008
00097564209	60763.93	930.2	0.064 ± 0.010
00098285001	60768.75	2246.7	0.024 ± 0.004
00098285005	60783.46	205.6	0.022 ± 0.005
00098285004	60783.78	2795.8	0.048 ± 0.005
00098285008	60798.47	190.5	0.055 ± 0.042
00098285009	60798.47	476.3	0.097 ± 0.031
00098285007	60798.89	2640.2	0.015 ± 0.003

Notes: ^a Modified Julian Date. The count rates were measured in the 0.3 – 10.0 keV.

the same data as Fig. 1, but zoomed in from MJD 59500.0 onward to more clearly highlight the pre-eruption dip. Following Merc et al. (2025), the AAVSO light curves have been cleaned of outliers and averaged over 1-day intervals. The Swift/UVOT UVW2 light curve is included for reference only. The Swift/BAT hard X-ray light curve has been averaged over 20-day intervals for clarity in visual presentation.

3.1.1. Characteristics of the high state

Following the last nova eruption, T CrB remained in a quiescent state until 2014, when it underwent a sudden optical brightening. The mass accretion rate increased abruptly by approximately a factor of 20 over quiescent levels (Schaefer 2023a), reaching $2\text{--}6 \times 10^{-8} M_{\odot}\text{yr}^{-1}$ (Luna et al. 2018; Zamanov et al. 2023; Schaefer 2023a; Toalá et al. 2024). This transition was accompanied by notable changes across the electromagnetic spectrum.

In X-rays, the hard component ($E \geq 2$ keV) diminished, while a soft component ($E \leq 0.6$ keV) emerged, indicating that the boundary layer between the WD and the inner accretion disc (AD) had become optically thick (Luna et al. 2018, 2019). In the optical regime, the emergence and strengthening of high-ionization emission lines, along with a blue continuum, were observed (Munari et al. 2016). The mean B -band brightness increased by 0.9 mag, deviating from the typical ellipsoidal modulation (Planquart et al. 2025). The rising continuum corresponds to a hot component with an effective temperature of 9400 ± 500 K (Zamanov et al. 2023). A simultaneous radio flux enhancement, attributed to bremsstrahlung emission from ionized circumstellar material, was also detected (Linford et al. 2019).

These multi-wavelength indicators confirmed the onset of a pronounced high state (Munari et al. 2016), during which an estimated $\sim 2 \times 10^{-7} M_{\odot}$ was accreted onto the WD (Zamanov et al. 2023). This accumulation may be sufficient to trigger a thermonuclear runaway, with the next nova eruption predicted around 2025.5 ± 1.3 (Schaefer 2023a).

The amplitude of the brightening in the active state is smaller in the V band than in the B band (Merc et al. 2025). Moreover, at optical wavelengths, the shorter the wavelength, the greater the increase in flux compared to quiescence (Munari et al. 2016; Zamanov et al. 2016; Schaefer 2023a; Merc et al. 2025). Thus, enhanced activity during the high state is most pronounced at the bluest optical bands.

The high state is fundamentally driven by a sharp increase in the mass transfer rate from the donor star (Ilkiewicz et al. 2016). The accretion rate directly governs the optical depth of the boundary layer: higher \dot{M} leads to a transition from an optically thin to optically thick regime (Luna et al. 2018). This shift results in decreased X-ray flux and enhanced optical/UV emission. After early 2014, the boundary layer in T CrB became predominantly optically thick, likely representing the highest accretion rate ever recorded in the system (Luna et al. 2018).

X-ray emission in symbiotic binaries such as T CrB originates from the boundary layer between the WD and the AD (Luna et al. 2013, 2018; Zhekov & Tomov 2019). Disk instabilities can cause large amounts of material to be dumped onto the WD over short timescales, resulting in an optically thick layer and marking the onset of enhanced activity (Zhekov & Tomov 2019). The current high state is therefore attributed to a sustained increase in \dot{M}_{WD} (Luna et al. 2020; Zamanov et al. 2023).

Throughout this period, the evolution of X-ray flux was strongly anti-correlated with the optical light curve, a relationship consistent with theoretical models of disk accretion in which higher accretion rates yield lower X-ray-to-optical flux ratios (Toalá et al. 2024). Thus, the observed optical brightening is most plausibly driven by increased accretion onto the WD (Luna et al. 2018; Linford et al. 2019). We agree with these interpretations.

During the high state, several individual optical brightness peaks were observed and independently confirmed by Luna et al. (2018); Munari (2023); Munari et al. (2024, 2025). In this study, however, we focus on the long-term average brightness trends. After accounting for the sinusoidal orbital modulation, the average B -band brightness increased by 0.9 mag compared to quiescence (Planquart et al. 2025). The average brightness increases in the V , R , and I bands were 0.38 mag, 0.22 mag, and 0.12 mag, respectively. As shown in Fig. 3, the dereddened $(B - V)_0$ color evolution of T CrB indices remain relatively blue during the 2014–2023 high state, reflecting a significant contribution from hot accretion-driven emission. The average $(B - V)_0$ in quiescence is 1.41 ± 0.04 , whereas during the high state it decreases to 0.93 ± 0.02 .

Soon after reaching the brightness maximum during the high state, T CrB began a slow and steady descent in the B band and U band (Munari et al. 2025). As shown in Fig. 4, following the initial brightening in the B band, the average brightness gradually declined throughout the remainder of the high state. This decline is anti-correlated with the X-ray emission in the 0.3–10 keV range (see Fig. 1).

X-ray count rates in the 0.3–10 keV band provide additional support for this inverse relationship. On 2005.46, the count rate was 0.092 ± 0.003 ; it increased slightly to 0.109 ± 0.003 on 2005.78 and remained high at 0.102 ± 0.003 on 2008.20. However, it declined to 0.071 ± 0.004 by 2011.92, 0.054 ± 0.003 by 2015.73, and reached a minimum of 0.012 ± 0.001 in 2017. This steady decline, apart from the slight early rise, spans more than a decade and coincides with the system's optical brightening, reinforcing the observed anti-correlation between optical and X-ray flux.

In the UV bands, a similar trend is evident. Between 2008.20 and 2011.92, the average UVW1 (2600 Å) magnitude increased by 0.13 mag, and the UVM2 (2246 Å) magnitude by 0.09 mag, without accounting for orbital modulation. During the 2005–2013 quiescent phase, the B-band light curve of T CrB exhibits a slow but measurable increase in brightness at a rate of $\Delta B = -0.04 \text{ mag yr}^{-1}$ (Munari et al. 2025). As shown in Fig. 4, the B-band brightness does not increase monotonically over this interval, but rather displays gradual fluctuations with alternating rises and declines. In contrast, the AAVSO light curves in the V, R, and I bands over the same period (2005–2013) do not exhibit a consistent upward trend (see Fig. 4). These results imply that UV and B-band flux is more variable and possibly anti-correlated with X-ray emission even during quiescence. Moreover, shorter wavelengths exhibit more pronounced variability, suggesting greater sensitivity to accretion-related changes.

From 2008.20 through the high state, the average brightness in the UVW1 band increased by 3.01 mag, and by 4.60 mag in the UVM2 band. Like the optical bands, UV brightness increased more strongly at shorter wavelengths, highlighting a consistent pattern across the spectrum during the transition from quiescence to the active state.

As shown in Fig. 1, the 0.3–3 keV X-ray count rates were relatively high and stable during 2017.05–2017.83 but remained low for the rest of the high state. Consequently, the hardness ratio (3–10 keV / 0.3–3 keV) primarily reflects variability in the 3–10 keV range and tracks closely with its evolution.

Since the onset of optical brightening, the X-ray spectrum has softened significantly. The hardness ratio (2–10 keV / 0.3–2 keV) declined by nearly two orders of magnitude by early 2018 (Luna et al. 2018). On 2018 January 30, the X-ray emission was harder than on 2017 February 23 (Zhekov & Tomov 2019). During 2017.05–2017.83, the hardness ratio remained low (0.10–3.24), but gradually increased through 2021.64, and again between 2022.18 and 2022.60 (see Fig. 1).

The Swift/BAT hard X-ray (15–50 keV) light curve shows minimal flux during 2017.05–2017.83, followed by a gradual increase. This pattern closely resembles the evolution of the 3–10 keV X-ray light curve, further emphasizing the consistent multi-band behavior during the high state.

3.1.2. Properties of the pre-eruption dip state

The 2023–2024 pre-eruption dip marks the most significant multi-wavelength transition observed in T CrB over the past eight decades. Its onset around MJD 60050 (April 2023) coincided with the decline from the prolonged 2014–2023 high state. The fading proceeded steadily over ≈ 130 days, reaching minimum brightness near MJD 60180 (August 2023).

During the pre-eruption dip in 2023–2024, the ellipsoidal variation in the B-band light curve became more clearly defined compared to the preceding high state. This modulation subsequently diminished after the dip phase.

Although the timing of the optical brightness minimum during the pre-eruption dip has been reported by Munari et al. (2024, 2025), this study focuses on the average brightness across the dip. We compute the average magnitudes over a 113.79-day interval (MJD 60253.105–60366.895), corresponding to half the orbital period (227.58 days), centered on the bottom of the dip.

The average brightness decreased by the following amounts (after accounting for orbital modulation): 1.364 mag in the *U* band, 0.738 mag in *B*, 0.293 mag in *V*, 0.148 mag in *R*, and 0.074 mag in *I*. This wavelength-dependent fading is consistent with

a color-dependent decline, most prominent in the *B* band and progressively smaller at longer wavelengths (Schlindwein et al. 2025). A pronounced reddening develops during the 2023–2024 pre-eruption dip, with $(U - B)_0$ showing the largest change (see Fig. 3), and an average $(B - V)_0$ of 1.33 ± 0.02 during the dip. In the UV, the average brightness declined by 2.533 mag in the UVM2 band and 2.146 mag in UVW1, again considering the sinusoidal modulation at half the orbital period.

Interestingly, the average *V*-band brightness during the dip remained ~ 0.087 mag above the typical quiescent level. Similar small excesses above quiescence were also observed in the *I* (0.046 mag), *R* (0.072 mag), *B* (0.162 mag), and UV bands.

As illustrated in Figs. 1 and 2, the 0.3–10 keV X-ray count rate generally increased during the fading phase of the pre-eruption dip (from its onset to the optical minimum), consistent with the findings of Munari et al. (2024) that reported a steady rise in X-ray flux at the end of the high state. Subsequently, the count rate decreased during the post-dip recovery phase (from the optical minimum to the end of the dip).

The 0.3–10 keV X-ray light curve exhibits an "outburst-like" profile with three peaks during the pre-eruption dip. Notably, these peaks do not coincide with the maxima expected from sinusoidal modulation (i.e., phase = 0.25), suggesting intrinsic variability. The three peaks are present in both the 0.3–3 keV and 3–10 keV light curves, but the 3–10 keV band exhibits larger amplitude variations. Consequently, the hardness ratio increases and then decreases, producing a peak-like evolution during this interval. A similar peak-shaped trend is observed in the 15–50 keV hard X-ray light curve.

Throughout the pre-eruption dip, both the soft (0.3–10 keV) and hard (15–50 keV) X-ray light curves exhibit an anti-correlated relationship with the optical and UV brightness. Furthermore, the amplitude of the brightness decline across the optical and UV bands increases with decreasing wavelength, emphasizing the color-dependent nature of the dip.

After the minimum of the 2023–2024 dip, both $(B - V)_0$ and $(U - B)_0$ gradually trend back toward bluer values, although neither returns to the high-state levels; a smaller but distinct reddening episode is again present. As illustrated in Fig. 1 and Fig. 2, a second, lower-amplitude dip is visible in the UV bands between September 2024 and February 2025, hereafter referred to as the "second dip," following the main pre-eruption dip. Although the sampling is sparser, both the UVW1 and UVM2 bands show declines of ≈ 0.8 –1.1 mag relative to the preceding maximum, while the *B* band exhibits a modest ~ 0.25 mag decrease. The event lasted for ~ 150 days, comparable to roughly half an orbital cycle, despite a gap in Swift coverage during this interval. In contrast to the pronounced reddening that developed during the 2023–2024 pre-eruption dip, a smaller secondary reddening is also apparent during the 2024–2025 dip. This repetition indicates that the feature is intrinsic to the system rather than an artifact of orbital sinusoidal modulation.

3.2. Timing analysis

We applied the Lomb-Scargle periodogram (LSP) method (Scargle 1982) to search for periodicities in the X-ray light curves of T CrB. Specifically, we used the lomb package developed by Thomas Ruf⁵, which computes the LSP for unevenly sampled time series.

We separately analyzed the XRT light curves in the 0.2–0.6 keV, 0.3–3 keV, 3–10 keV, and 0.3–10 keV energy bands. No

⁵ <https://cran.r-project.org/web/packages/lomb/index.html>

statistically significant periodicity was detected in any of these energy ranges. We did not expect to recover the previously reported 6000–6500 s periodic variability in the 0.2–0.6 keV band (Zhekov & Tomov 2019) using Swift/XRT, as these periods are too close to Swift’s orbital period of 5754 s.

The Swift/BAT hard X-ray transient monitor has been detecting T CrB since 15 February 2005. We analyzed the BAT light curves in the 15–50 keV band spanning from 15 February 2005 (MJD 53416) to 20 July 2025 (MJD 60876), covering approximately 32.78 cycles of the 227.58-day orbital period and 65.56 cycles of the ellipsoidal modulation period. Neither the orbital period nor the ellipsoidal modulation period was detected in the orbital- or daily-binned light curves.

4. Discussion

Our analysis builds upon earlier works (Luna et al. 2018, 2020; Zhekov & Tomov 2019) by extending the Swift and AAVSO monitoring of T CrB through 2025. This 20-year dataset captures the full evolution of the system, from quiescence to the 2014–2023 high state and into the 2023–2025 pre-eruption dip sequence. The continuous multi-band coverage allows a quantitative characterization of the anti-correlation between optical/UV and X-ray fluxes and of the wavelength-dependent amplitudes of both brightening and fading. In contrast to previous studies that focused primarily on the 2014–2015 high state, we identify a new, secondary dip in late 2024 and demonstrate that the anti-correlation persists even during this later stage. Additionally, we present the first long-term dereddened color evolution of T CrB over two decades. These results provide a unified picture in which both the high and dip states are manifestations of variable mass-accretion rates and changing optical depth of the boundary layer.

The increase in optical brightness from quiescence to the high state is likely driven by an enhanced accretion rate (Luna et al. 2018; Linford et al. 2019). Similarly, the corresponding increase in UV brightness from quiescence to the high state may also be attributed to enhanced accretion onto the WD.

Schaefer (2023a) suggested that a pre-eruption dip similar to the one observed before the 1946 outburst could serve as an indicator of an impending nova, with the eruption expected about a year after the dip onset. In March–April 2023, T CrB began fading, which was interpreted as a potential pre-eruption dip (Schaefer et al. 2023; Toone 2023), and based on this, an eruption was predicted for around 2024.4 ± 0.3 . However, outburst has not occurred yet. Merc et al. (2025) found that the decline in the *B*-band during the 2023–2024 pre-eruption dip closely resembled that seen before the 1946 eruption, while the behavior in the *V*-band differed. During this recent dip, no deep decline occurred in the *V*-band; instead, the system returned to a typical quiescent level before re-brightening (Merc et al. 2025). Our analysis shows that the average brightness during the 2023–2024 dip remains higher than the historical quiescent level in both optical (*I*, *R*, *V*, *B*) and UV bands.

The 1946 pre-eruption dip, observed about 1 year before the outburst, featured a dramatic decline in the *V* band—over 1.5 mag below the expected brightness of the red giant itself—suggesting an external obscuration mechanism. Schaefer (2023a) proposed circumstellar dust as the most plausible explanation. However, this hypothesis is challenged by the lack of stronger dimming at shorter (bluer) wavelengths, contrary to standard extinction laws. Alternative explanations have been considered. Zamanov et al. (2024) proposed the formation of a dense envelope (~ 1000 –2000 km in radius) around the WD

prior to the 1946 eruption. While this model could account for brightness declines, it fails to explain the magnitude of the dimming in the *V* band during the 2023–2024 pre-eruption dip state. Additionally, it cannot account for the anti-correlated rise in X-rays seen during the 2023–2024 event.

Munari et al. (2024) argued that the 2023–2024 dip was due to intrinsic variations in the brightness of the accretion disk rather than obscuration. They noted that the red giant’s contribution dominated the system’s light during this phase, and the accretion disk contributed negligibly. Our findings—showing clearer ellipsoidal modulation in the *B* band and above-quiescence brightness levels—support this interpretation, implying that external dust obscuration may not be necessary to explain the dip. The *B*-band emission is primarily produced by the accretion disk and irradiation of the red giant by the WD. Therefore, a decrease in accretion rate leads to a corresponding decline in energy output from the disk (Stoyanov et al. 2025).

The first X-ray detection of T CrB was made with the Einstein observatory (Cordova et al. 1981), with subsequent studies conducted using multiple X-ray missions (Swift, RXTE, XMM-Newton, NuSTAR, and Suzaku) over the past two decades. T CrB exhibits hard and heavily absorbed X-ray emission (Luna et al. 2008; Kennea et al. 2009; Ilkiewicz et al. 2016; Luna et al. 2018; Zhekov & Tomov 2019), making it a typical member of the δ -type X-ray symbiotic stars. In these systems, X-rays are thought to originate from the boundary layer between the accretion disk and the WD (Luna et al. 2013, 2018). T CrB also shows strong X-ray flickering (minute-scale stochastic variability) in both soft (< 10) and hard (> 10 keV) X-rays (Luna et al. 2008; Ilkiewicz et al. 2016), consistent with accretion-driven processes. Boundary layer plasma temperatures showed dramatic changes from the quiescent state to the high state, that attributes to variations in mass accretion rate (Toalá et al. 2024).

The observed anti-correlation between optical/UV and X-ray brightness, combined with a wavelength-dependent decline in brightness, parallels the behavior seen during the high state. Therefore, the pre-eruption dip may share the same underlying mechanism: variability in the mass accretion rate (see Sect. 3.1.1). In this framework, the fading phase corresponds to a decline in \dot{M} , leading to lower optical/UV brightness and a transition to an optically thinner boundary layer—resulting in increased X-ray emission. This transition explains the observed anti-correlation between optical/UV and X-ray brightness throughout the dip. Conversely, the recovery phase marks a rise in \dot{M} , brightening the optical/UV bands while X-rays decline as the boundary layer becomes optically thick again.

The presence of three peaks in the 0.3–10 keV X-ray light curve during the pre-eruption dip cannot be explained by orbital modulation or simple flickering. Instead, they are likely manifestations of variable mass accretion onto the WD, possibly triggered by disk instabilities or magnetic channeling.

During the high state, the structure of the boundary layer changed dramatically, consistent with a disk instability event responsible for the observed optical brightening (Luna et al. 2018). If the pre-eruption dip arises from the same physical mechanism as the high state, then the boundary layer may have undergone a similar or even more pronounced transformation. The duration of the pre-eruption dip (~ 1.5 years), comprising both the fading and recovery phases, is comparable to the ~ 2 -year optical brightening phase of the high state, further supporting this analogy.

The 2023–2024 pre-eruption dip may represent a pivotal stage in T CrB’s long-term evolution toward eruption. The depth

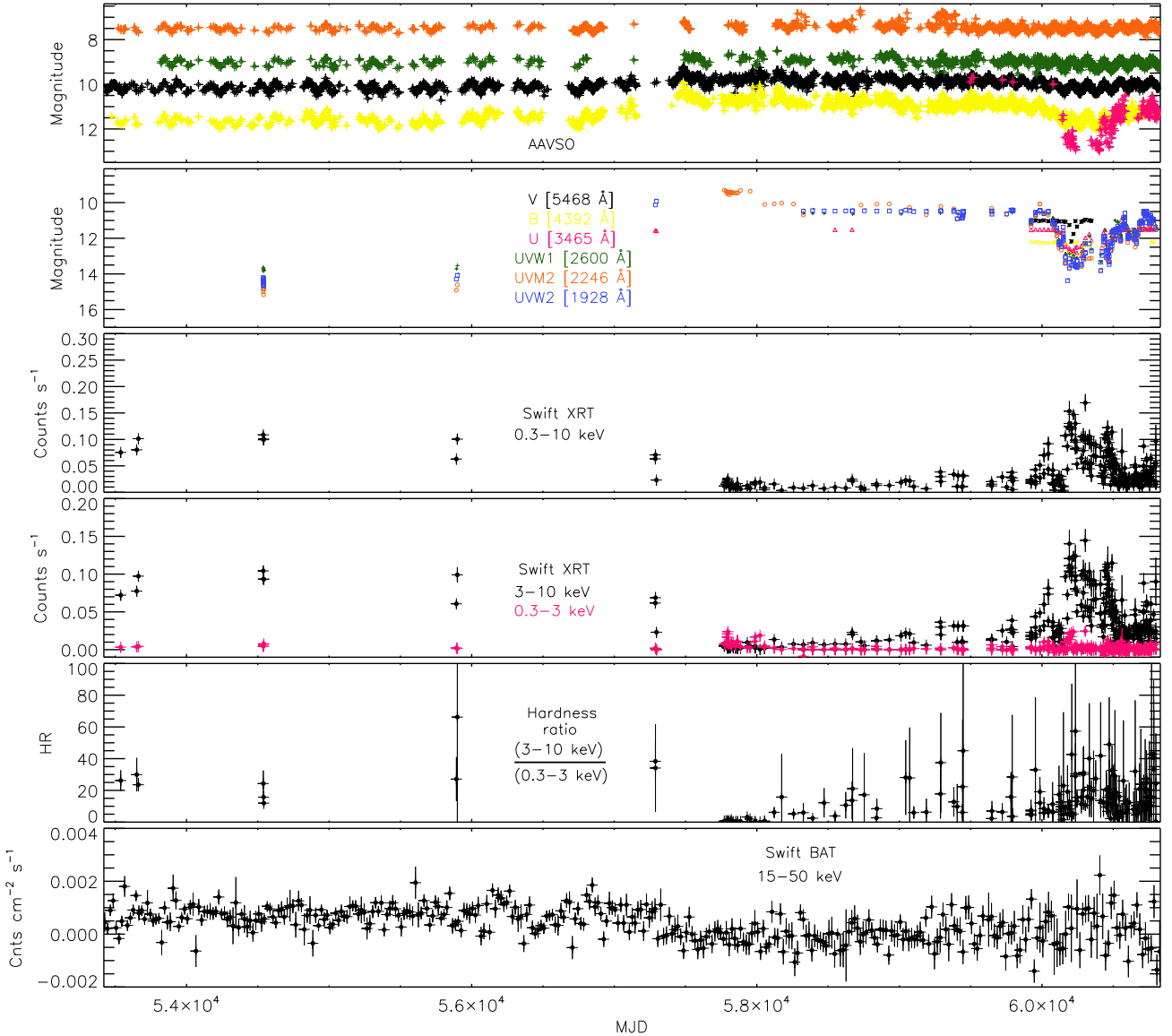


Fig. 1. From top to bottom: AAVSO light curves of T CrB from early 2005 to early 2025 in the following bands: I (green), R (orange), V (black), B (yellow), and U (red). Subsequent panels display: Swift/UVOT light curves in multiple filters; Swift/XRT 0.3 – 10 keV light curve (PC mode); Swift/XRT light curves in 3 – 10 keV (black) and 0.3 – 3 keV (red); X-ray hardness ratio (3 – 10 keV / 0.3 – 3 keV); and the Swift/BAT light curve.

of the dip increases systematically toward shorter wavelength indicates that the fading originates from the hot accretion component rather than from circumstellar extinction. Simultaneously, both the 0.3–10 keV and 15–50 keV X-ray fluxes rose sharply, producing a pronounced anti-correlation with the optical/UV light curves. Such behavior is consistent with a reduction in the accretion rate leading to a transition of the boundary layer from optically thick to optically thin emission.

Furthermore, T CrB’s evolution in the X-ray hardness–intensity diagram (HID) resembles that of black hole binaries, accreting neutron stars, and active galactic nuclei (AGN), following hard state → hard-intermediate state (HIMS) → soft-intermediate state (SIMS) → soft state → SIMS → HIMS → hard state (Toalá et al. 2024). However, during the 2023–2024 dip, T CrB deviated from this pattern, suggesting that the nova eruption may be imminent.

The second dip from September 2024 to February 2025 (following the primary pre-eruption dip) cannot be fully attributed to orbital modulation, it may share a similar formation mechanism—likely tied to variations in accretion rate. The correlated UV–optical behavior, the distinct reddening of $(B - V)_0$, and the simultaneous increase in soft-X-ray flux suggest that this second dip is not due to geometric obscuration but rather reflects a renewed, short-term reduction of the accretion rate and a temporary return to an optically thinner boundary layer. Its occurrence shortly after the main 2023–2024 dip indicates that the system may be undergoing a sequence of thermal–viscous instabilities in the inner disk as the white dwarf envelope approaches critical ignition conditions.

Therefore, the 2023–2025 dips is not merely a photometric fluctuation but a critical diagnostic of pre-nova accretion physics. Its detailed characterization provides the first modern observational counterpart to the fading recorded before the

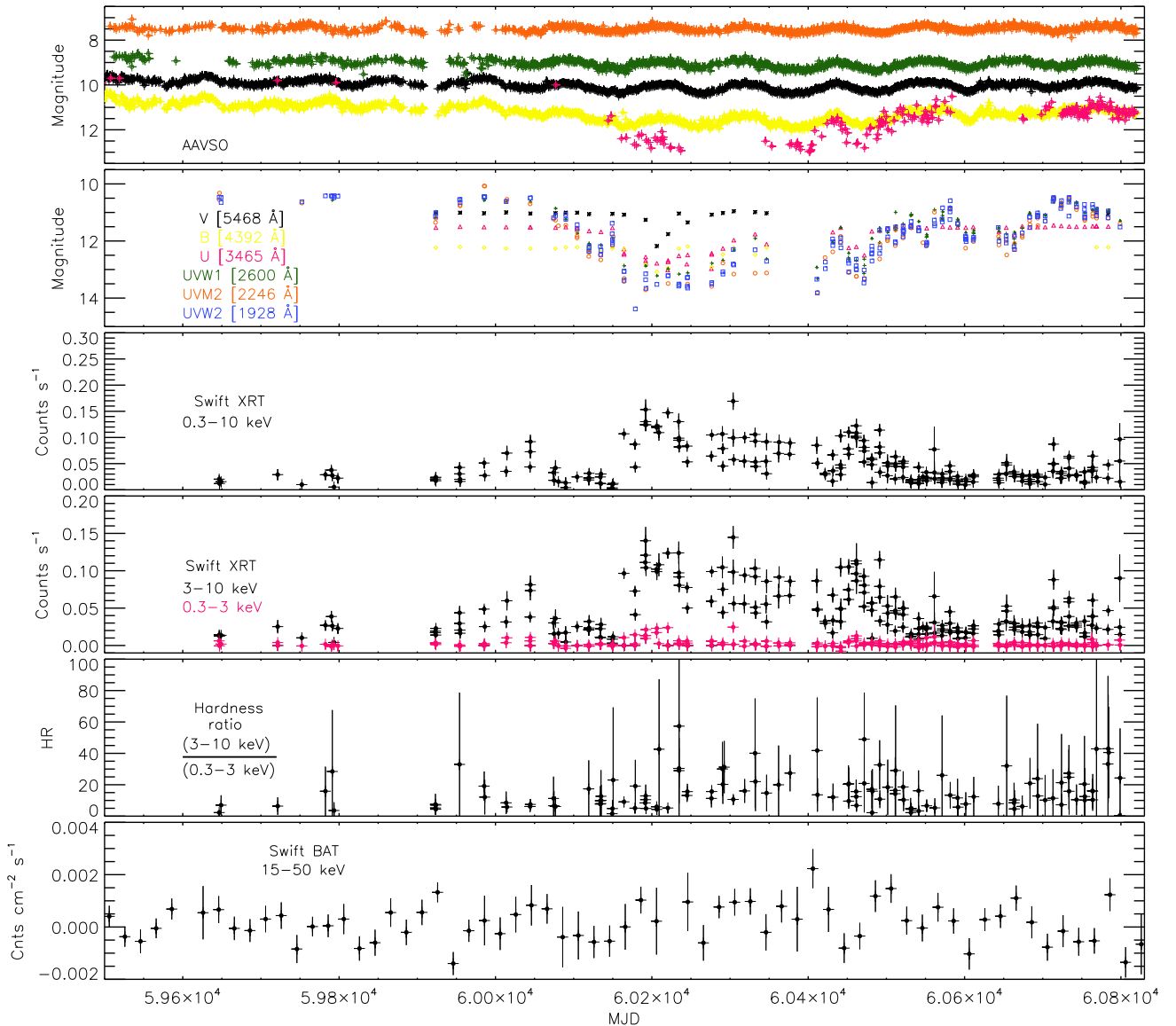


Fig. 2. From top to bottom: AAVSO light curves of T CrB from late 2021 to early 2025 in the following bands: I (green), R (orange), V (black), B (yellow), and U (red). Subsequent panels display: Swift/UVOT light curves in various filters; the Swift/XRT 0.3 – 10 keV light curve (PC mode); Swift/XRT light curves in 3 – 10 keV (black) and 0.3 – 3 keV (red); the X-ray hardness ratio (3 – 10 keV / 0.3 – 3 keV); and the Swift/BAT light curve.

1946 eruption. Taken together, these properties indicate that the pre-eruption dip represents a critical readjustment in the mass-transfer process as the system approaches thermonuclear runaway—analogous to, but more complex than, the fading recorded prior to the 1946 eruption. The dips therefore provide a valuable empirical probe of the conditions immediately preceding a nova outburst in a symbiotic recurrent system.

The sustained enhancement of the accretion rate to $\dot{M} \approx (2\text{--}6) \times 10^{-8} M_{\odot} \text{ yr}^{-1}$ since 2014 implies that over the last decade the white dwarf has accumulated $\gtrsim (1\text{--}2) \times 10^{-7} M_{\odot}$ of fresh material. For a near-Chandrasekhar-mass ($1.37 M_{\odot}$) white dwarf, this envelope mass is sufficient to trigger thermonuclear runaway within a few years (Hachisu & Kato 2001; Wolf et al. 2013; Hillman et al. 2015, 2020). The observed pre-eruption dips can therefore be interpreted as phases of temporarily reduced mass transfer as the disk and boundary layer re-adjust to the accumulating pressure in the WD envelope. The corresponding in-

crease in X-ray emission during the dips marks the transition to a thinner, hotter boundary layer, consistent with the behavior expected immediately before runaway ignition. Thus, the photometric and spectroscopic evolution of T CrB in 2023–2025 provides empirical evidence that the system is entering the final pre-nova stage. Given the significant structural and photometric changes observed during the 2023–2024 pre-eruption dip, including changes in the accretion rate and boundary layer, and the consensus in the literature predicting an imminent nova eruption, the likelihood that this dip is unrelated to the upcoming outburst is low.

5. Summary and Conclusions

We present a comprehensive multi-wavelength study of the symbiotic RN T CrB, utilizing Swift (XRT/BAT/UVOT) and AAVSO observations spanning 2005–2025. This time frame

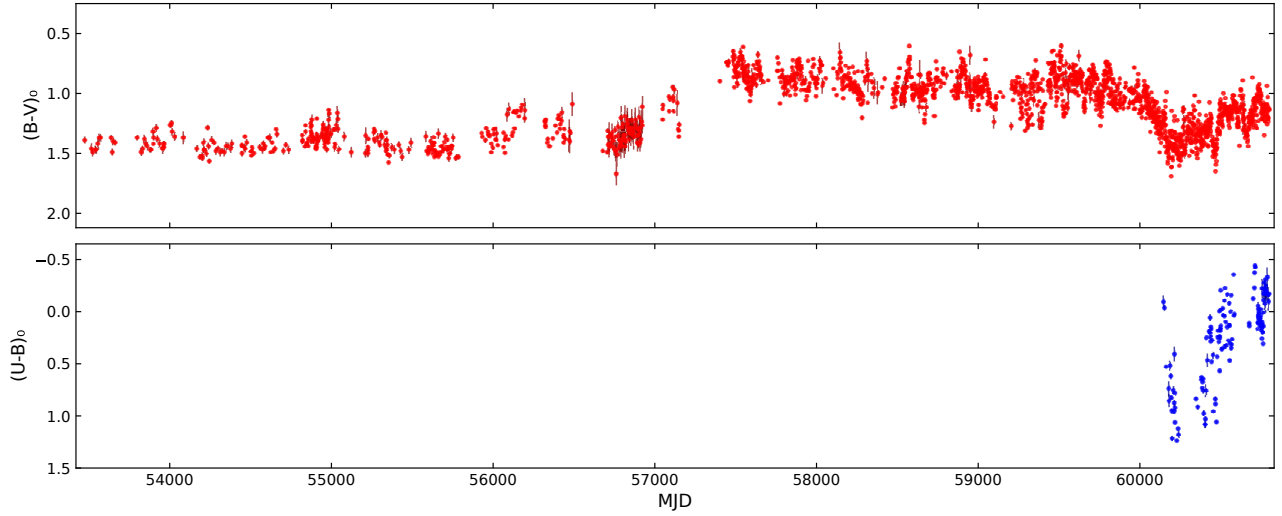


Fig. 3. Dereddened color evolution of T CrB from early 2005 to early 2025 based on AAVSO photometry. The top panel shows $(B - V)_0$ (red) and the bottom panel shows $(U - B)_0$ (blue). Colors were computed from near-simultaneous (± 0.25 d) AAVSO UBV measurements, adopting $E(B - V) = 0.07$ (Nikolov 2022). For clarity, the dereddened color indices were averaged in 1-day bins.

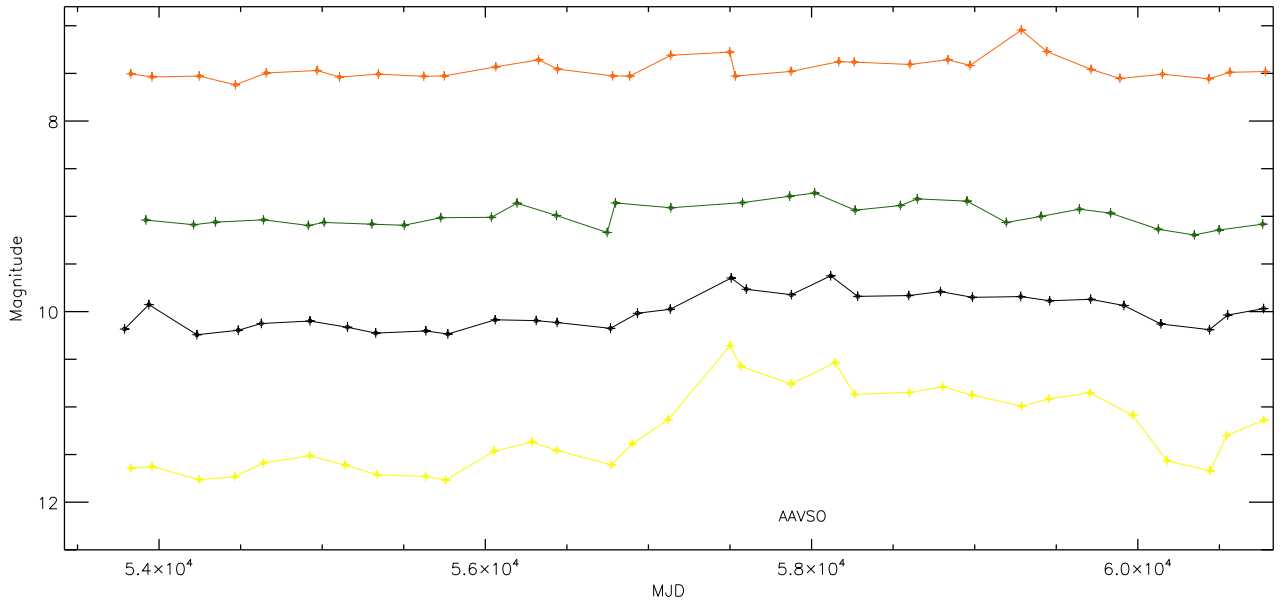


Fig. 4. AAVSO light curves of T CrB from 2005.78 to early 2025 in the I (green), R (orange), V (black), and B (yellow) bands. The data have been averaged over 227.58-day intervals, corresponding to the orbital period (Planquart et al. 2025).

covers the system's quiescent phase, the high state, and the recent pre-eruption dip. The principal findings and conclusions of our work are as follows.

Analysis of the optical light curves in the I, R, V, and B bands confirms that the amplitude of brightening during the initial optical brightening of the high state is wavelength-dependent: the shorter the wavelength, the greater the flux increase relative to quiescence. A similar trend is evident in the UV bands, where shorter wavelengths exhibit more significant variability than longer wavelengths, both within the UV domain and when compared to the optical. We also find evidence suggesting that the UV emission is anti-correlated with the X-ray flux even during the quiescent state. During the high state, X-ray fluxes in both the 0.3–10 keV and 15–50 keV bands rose gradually after

reaching a minimum in 2017. The B-band light curve remained anti-correlated with the X-rays beyond the initial optical brightening, supporting a scenario driven by variations in the accretion rate.

We find that the average optical and UV brightness levels during the bottom of the pre-eruption dip remained above those of the quiescent state. Throughout the entire pre-eruption dip, the brightness change in the optical and UV bands was more pronounced at shorter wavelengths. Furthermore, X-rays in both soft (0.3–10 keV) and hard (15–50 keV) bands were anti-correlated with the optical and UV emission during the entire pre-eruption dip. The presence of three peaks in the soft X-ray light curve during the dip likely reflects short-term fluctuations in the accretion rate. Following the main pre-eruption dip, a sec-

ond, lower-amplitude dip was observed in the UV band between September 2024 and February 2025. Notably, no such secondary dip was observed after the pre-eruption dip of the 1946 outburst.

The pre-eruption dip (2023–2024) may have resulted from a decrease in the accretion rate, accompanied by a substantial transformation of the boundary layer. The observed variability across all bands suggests a transition from an optically thick to an optically thin boundary layer—mirroring the mechanism thought to drive the earlier high brightening phase. These results imply that the dip was not an isolated phenomenon, potentially heralding an imminent nova eruption.

The absence of modulation at either the orbital or ellipsoidal periods in the 15–50 keV hard X-ray light curves supports the interpretation that the hard X-ray emission arises from the compact boundary layer between the WD and the inner accretion disc, rather than from extended structures associated with the red giant or the wider binary geometry.

The 2023–2024 dip exhibits notable similarities with the pre-eruption behavior observed prior to the 1946 nova outburst. The subsequent recovery in brightness likely reflects resumed mass accumulation. Continued monitoring in the UV and X-ray bands, particularly during any forthcoming supersoft X-ray phase, will be essential to test the accretion-variation scenario.

This study presents the continuous 20-year, multi-wavelength record of T CrB encompassing quiescent, high, and pre-eruption dip phases. The analysis reveals two consecutive dips (2023–2024 and 2024–2025) characterized by wavelength-dependent fading and anti-correlated X-ray brightening, both consistent with temporary reductions in the accretion rate. The persistence of these transitions, together with the inferred accumulated envelope mass on the near-Chandrasekhar white dwarf, supports the interpretation that T CrB is approaching a thermonuclear runaway. These results establish a coherent accretion-variation framework linking the high and dip states and provide the comprehensive pre-eruption view yet obtained of a symbiotic recurrent nova on the verge of outburst.

Overall, T CrB’s sequence of brightening and fading episodes highlights the key role of accretion variations in modulating emission across the optical, UV, and X-ray regimes. The system provides a rare opportunity to investigate pre-eruption dynamics in long-period WD binaries. Future multi-wavelength observations, spanning from γ -rays to radio, during the anticipated nova eruption will offer a unique means to constrain the evolution of the accretion rate and to further advance our understanding of RN physics.

6. Data availability

The Swift data presented in this article were obtained from the Mikulski Archive for Space Telescopes (MAST) at the Space Telescope Science Institute. The specific observations analyzed can be accessed via [doi: 10.17909/h2jm-m826]<https://doi.org/10.17909/h2jm-m826>.

Acknowledgements

We extend our gratitude to observers worldwide for their valuable contributions to the AAVSO database. Additionally, this research utilized data provided by the UK Swift Science Data Centre at the University of Leicester. This work is supported by the High-level Talents Research Start-up Fund Project of Liupanshui Normal University (Grant No. LPSSYKYJJ202208), the Science and Technology Foundation

of Guizhou Province (Grant No. QKHJC-ZK[2023]442), the Discipline-Team of Liupanshui Normal University (Grant No. LPSSY2023XKTD11), the Liupanshui Science and Technology Development Project (Grant No. 52020-2024-PT-01), the National Natural Science Foundation of China (Grant No. 12303054, 12393853, 12003020), the National Key Research and Development Program of China (Grant No. 2024YFA1611603), the Yunnan Fundamental Research Projects (Grant Nos. 202401AU070063, 202501AS070078), and the International Centre of Supernovae, Yunnan Key Laboratory (No. 202302AN360001), the Shaanxi Fundamental Science Research Project for Mathematics and Physics (Grant No. 23JSY015). RZS acknowledges the support from the China Postdoctoral Science Foundation (Grant No. 2024M752979).

References

Bailer-Jones, C. A. L., Rybizki, J., Fouesneau, M., Demleitner, M., & Andrae, R. 2021, AJ, 161, 147

Bailey, J. 1975, Journal of the British Astronomical Association, 85, 217

Barthelmy, S. D., Barbier, L. M., Cummings, J. R., et al. 2005, Space Sci. Rev., 120, 143

Belczynski, K. & Mikolajewska, J. 1998, MNRAS, 296, 77

Burrows, D. N., Hill, J. E., Nousek, J. A., et al. 2005, Space Sci. Rev., 120, 165

Cordova, F. A., Mason, K. O., & Nelson, J. E. 1981, ApJ, 245, 609

Fekel, F. C., Joyce, R. R., Hinkle, K. H., & Skrutskie, M. F. 2000, AJ, 119, 1375

Gehrels, N., Chincarini, G., Giommi, P., et al. 2004, ApJ, 611, 1005

Hachisu, I. & Kato, M. 2001, ApJ, 558, 323

Hillman, Y., Prialnik, D., Kovetz, A., & Shara, M. M. 2015, MNRAS, 446, 1924

Hillman, Y., Shara, M. M., Prialnik, D., & Kovetz, A. 2020, Nature Astronomy, 4, 886

Hinkle, K. H., Nagarajan, P., Fekel, F. C., et al. 2025, ApJ, 983, 76

Ikiewicz, K., Mikołajewska, J., Stoyanov, K., Manousakis, A., & Miszalski, B. 2016, MNRAS, 462, 2695

Ikiewicz, K., Mikołajewska, J., & Stoyanov, K. A. 2023, ApJ, 953, L7

Kennea, J. A., Mukai, K., Sokoloski, J. L., et al. 2009, ApJ, 701, 1992

Krimm, H. A., Holland, S. T., Corbet, R. H. D., et al. 2013, ApJS, 209, 14

Kuin, N. P., Luna, G. J. M., Page, K., et al. 2023, The Astronomer’s Telegram, 16114, 1

Linford, J. D., Chomiuk, L., Sokoloski, J. L., et al. 2019, ApJ, 884, 8

Liu, D., Wang, B., Ge, H., Chen, X., & Han, Z. 2019, A&A, 622, A35

Luna, G. J. M., Mukai, K., Sokoloski, J. L., et al. 2018, A&A, 619, A61

Luna, G. J. M., Nelson, T., Mukai, K., & Sokoloski, J. L. 2019, ApJ, 880, 94

Luna, G. J. M., Sokoloski, J. L., & Mukai, K. 2008, in Astronomical Society of the Pacific Conference Series, Vol. 401, RS Ophiuchi (2006) and the Recurrent Nova Phenomenon, ed. A. Evans, M. F. Bode, T. J. O’Brien, & M. J. Darnley, 342

Luna, G. J. M., Sokoloski, J. L., Mukai, K., & M. Kuin, N. P. 2020, ApJ, 902, L14

Luna, G. J. M., Sokoloski, J. L., Mukai, K., & Nelson, T. 2013, A&A, 559, A6

Maslenikova, N. A., Tatarnikov, A. M., Tatarnikova, A. A., et al. 2023, Astronomy Letters, 49, 501

Merc, J., Wyrzykowski, Ł., Beck, P. G., et al. 2025, MNRAS, 541, L14

Munari, U. 2023, Research Notes of the American Astronomical Society, 7, 145

Munari, U., Dallaporta, S., & Cherini, G. 2016, New A, 47, 7

Munari, U., Ochner, P., Dallaporta, S., et al. 2024, The Astronomer’s Telegram, 16404, 1

Munari, U., Walter, F., Masetti, N., et al. 2025, A&A, 701, A176

Mürset, U. & Schmid, H. M. 1999, A&AS, 137, 473

Nikolov, Y. 2022, New A, 97, 101859

Page, M. J., Kuin, N. P. M., Breeveld, A. A., et al. 2013, MNRAS, 436, 1684

Planquart, L., Jorissen, A., & Van Winckel, H. 2025, A&A, 694, A85

Roming, P. W. A., Kennedy, T. E., Mason, K. O., et al. 2005, Space Sci. Rev., 120, 95

Sanford, R. F. 1949, ApJ, 109, 81

Scargle, J. D. 1982, ApJ, 263, 835

Schaefer, B. E. 2022, MNRAS, 517, 6150

Schaefer, B. E. 2023a, MNRAS, 524, 3146

Schaefer, B. E. 2023b, Journal for the History of Astronomy, 54, 436

Schaefer, B. E., Kloppenborg, B., Waagen, E. O., & Observers, T. A. 2023, The Astronomer’s Telegram, 16107, 1

Schlindwein, W., Baptista, R., & Luna, G. J. M. 2025, ApJ, 989, 78

Shahbaz, T., Somers, M., Yudin, B., & Naylor, T. 1997, MNRAS, 288, 1027

Stoyanov, K. A., M. Luna, G. J., Zamanov, R. K., et al. 2025, Bulgarian Astronomical Journal, 42, 29

Teyssier, F., Hinnefeld, J. D., Boussin, C., et al. 2023, The Astronomer's Telegram, 16109, 1

Toalá, J. A., González-Martín, O., Sacchi, A., & Vasquez-Torres, D. A. 2024, MNRAS, 532, 1421

Toone, J. 2023, British Astronomical Association Variable Star Section Circular, 196, 8

Wolf, W. M., Bildsten, L., Brooks, J., & Paxton, B. 2013, ApJ, 777, 136

Zamanov, R., Boeva, S., Latev, G. Y., et al. 2023, A&A, 680, L18

Zamanov, R., Semkov, E., Stoyanov, K., & Tomov, T. 2016, The Astronomer's Telegram, 8675, 1

Zamanov, R. K., Marchev, V., Marti, J., & Latev, G. Y. 2024, Bulgarian Journal of Physics, 51, 263

Zhekov, S. A. & Tomov, T. V. 2019, MNRAS, 489, 2930